J. Fluid Mech. (1992), *vol.* 244, *pp.* 583–604

Nonlinear three-wave interaction with non-conservative coupling

By DAVID W. HUGHES[1] AND MICHAEL R. E. PROCTOR[2]

[1] Department of Applied Mathematical Studies, The University, Leeds LS2 9JT, UK

[2] Department of Applied Mathematics and Theoretical Physics, University of Cambridge, Silver Street, Cambridge CB3 9EW, UK

(Received 7 March 1991 and in revised form 19 May 1992)

We consider the problem of three interacting resonant waves with arbitrary (non-conservative) nonlinear coupling. Such coupling arises naturally in the interaction of waves on shear flows, and in interactions between interfacial and gravity waves. We focus on the case where two modes are damped and have identical properties, and the third is linearly unstable. When the damping rates dominate the growth rate, the dynamics evolves on two disparate timescales and it is then possible to reduce the system to a multi-modal one-dimensional map, thus revealing clearly the complex sequence of bifurcations that occurs as the parameters are varied. We also investigate the effect on the equations of small additive noise; this can be simply modelled by a (deterministic) perturbation to the map. It is shown that even at very low levels, the effect of noise can be extremely important in determining the period and amplitude of the oscillations.

1. Introduction

The nonlinear development of wavelike instabilities of fluid flows depends critically on whether there are resonant couplings between modes with different spatial wavenumbers and frequencies (Weiland & Wilhelmsson 1977; Phillips 1981; Craik 1985). While general symmetry considerations require that non-resonant interactions between modes (for example, through alterations to the mean flow) typically appear at cubic order in the amplitude, resonant couplings can occur at quadratic order, and will thus dominate for small amplitudes. This is the case of three-wave resonance, which has generated an enormous literature in both the fields of fluid mechanics and plasma physics (see Craik 1985, and references therein). The majority of work has concentrated on the case where the quadratic interactions are conservative, and so do not affect the total energy of the flow. It is then natural (and indeed important) to ask, if one or more of the wave modes is linearly unstable, whether the presence of the quadratic interactions leads to bounded solutions even in the absence of cubic terms in the evolution equations. (Such a truncation of the full evolution equations can be justified when the moduli of all the linear growth and/or decay rates, and the amplitudes of the waves, are small.) It has been established that bounded solutions can certainly be found when just one of the three modes is unstable, and numerical studies in special cases have established that the dynamics is chaotic in certain parameter ranges (Wersinger, Finn & Ott 1980; Vyshkind & Rabinovich 1976). Hughes & Proctor (1990*a*) considered the case where the two stable eigenvalues are equal and the unstable eigenvalue has much smaller

growth rate. The system may then be reduced to a one-dimensional map, thus allowing the bifurcation structure to be extensively studied. They also showed that a small amount of additive noise can make a profound difference to the solutions.

Much less seems to be known about the case when the quadratic interactions are not conservative. This can happen, for example, in waves on shear flows, where the dissipative effects of critical layers are important (Craik 1971; see also Craik 1985), and in interactions between surface and internal gravity waves (Craik 1968). Because the underlying interaction problem, in the absence of any linear growth or decay terms, has no simple Hamiltonian structure it is very hard to make analytic progress. Neither are we aware of any numerical simulations, even in the symmetric case for which the two damped modes have identical properties, though Wang (1972) gives bounds on initial conditions for the solution to remain finite. Although the restriction to the symmetric case might seem special, it arises naturally in the contexts mentioned above, where the damped wave modes are of the same type (for example, in the shear flow problem the damped modes can be identified as two oblique waves making equal and opposite angles with the downstream direction). In the present paper we concentrate on it because of its relative simplicity; however, we have no reason to suppose that the complex transitions that we describe owe their existence solely to the symmetry. The study of the asymmetric problem presents an intriguing subject for future research.

The case of equal decay rates has also attracted attention since the equations turn out to be identical to those describing the interaction between two Hopf bifurcations with 2:1 resonance (Proctor & Hughes 1990). Knobloch & Proctor (1988) have investigated some aspects of the bifurcation structure, but did not conduct a systematic survey of parameter space; nor did they detect any chaotic solutions.

In the present paper we investigate the symmetric problem, with general quadratic interactions, in the same parameter range as Hughes & Proctor (1990*a*). Ideally we would like to treat a more physically realistic problem in which a continuous band of frequencies and wavenumbers interact. This is at present beyond the reach of analysis, and a full numerical solution has not to our knowledge been attempted. Our modelling of the effects of external noise can be considered as a first attempt to include the effects of the interaction with modes of nearby wavenumbers. A similar identification was made by Busse (1984) in his analysis of the Kuppers–Lortz instability of convection in a rotating layer. In what follows, we refrain from relating our results directly to a particular wave-interaction problem since to do so would suggest that the results were relevant to that problem alone. In contrast, we want to emphasize the universality of our work, and its applicability to many problems exhibiting similar symmetries. Such an approach has proved immensely fruitful in related fields, by emphasizing that the underlying symmetries of the problem have a profound effect on the bifurcation structure, while the influence of the physics can be reduced to the selection of particular cases (see e.g. Crawford & Knobloch 1991). Nonetheless, we shall attempt at every turn to relate the sometimes rather abstract results of our calculations to their manifestations in a real fluid.

It is now supposed that the basic flow state on which the waves occur is homogeneous in space and steady in time. Then any disturbance to this state can be decomposed into Fourier modes. We begin our analysis by assuming that the spatial resonance of the interacting modes is exact, while permitting a slight mismatch in the frequencies. Indeed, for the system with quadratic nonlinearities, the solutions blow up in finite time when the resonance is exact (McDougall & Craik 1991). Thus, if the

three disturbances are given by $C_j \exp(\mathrm{i}(\boldsymbol{k}_j \cdot \boldsymbol{x} - \omega_j t))$, $j = 1, 2, 3$, where the C_j are complex amplitudes then

$$\boldsymbol{k}_1 = \boldsymbol{k}_2 + \boldsymbol{k}_3; \quad \omega_1 = \omega_2 + \omega_3 + \Delta, \tag{1.1}$$

and the evolution equations are

$$\dot{C}_1 = \Gamma_1 C_1 + A_1 C_2 C_3 \exp(\mathrm{i}\Delta t), \tag{1.2a}$$

$$\dot{C}_{2,3} = -\Gamma_2 C_{2,3} - A_2 C_1 C^*_{3,2} \exp(-\mathrm{i}\Delta t), \tag{1.2b}$$

where the Γ_j are both supposed positive and the A_j are arbitrary non-zero complex constants. The substitution

$$C_1 = A_1 \exp(\mathrm{i}\Delta t)/A_1, \quad C_{2,3} = A_{2,3}/(|A_1 A_2|)^{\frac{1}{2}}, \tag{1.3}$$

simplifies (1.2) to

$$\dot{A}_1 = (\Gamma_1 - \mathrm{i}\Delta) A_1 + A_2 A_3 \mathrm{e}^{\mathrm{i}\Phi}, \tag{1.4a}$$

$$\dot{A}_{2,3} = -\Gamma_2 A_{2,3} - A^*_{3,2} A_1, \tag{1.4b}$$

where $\Phi \equiv \arg(A_1 A_2)$ is an arbitrary real constant. It is readily shown that $A_2 \to A_3 \mathrm{e}^{\mathrm{i}\lambda}$ exponentially, for some constant real λ, and that we may therefore identify A_2 and A_3 (after an appropriate shift in the origin of x). The further substitution

$$X = \Gamma_2^{-1} |A_1| \cos\phi, \quad Y = \Gamma_2^{-1} |A_1| \sin\phi, \quad Z = \Gamma_2^{-2} |A_2|^2, \tag{1.5}$$

where $\phi = \arg(A_1) - 2\arg(A_2)$ (see, for example, Vyshkind & Rabinovich 1976), leads to the system

$$\dot{X} = \gamma X + \delta Y - 2Y^2 + Z\cos\Phi, \tag{1.6a}$$

$$\dot{Y} = \gamma Y - \delta X + 2XY + Z\sin\Phi, \tag{1.6b}$$

$$\dot{Z} = -2Z(1+X), \tag{1.6c}$$

where time has been scaled with Γ_2^{-1}, $\gamma = \Gamma_1/\Gamma_2$ and $\delta = \Delta/\Gamma_2$.

Though this reduction to three real equations is computationally convenient, it undoubtedly obscures the relationship with the actual complex amplitudes. In what follows it must be borne in mind that both X and Y refer to the dominant (linearly unstable) A_1 mode, while Z is a measure of the (squared) amplitude of the damped modes.

In this paper we shall analyse equations (1.6) for the case of $0 < \gamma \ll 1$. Since the dynamics depends on δ and Φ only through their product we may, without loss of generality, restrict our attention to positive values of δ. When γ is small, there are two timescales present in the dynamics. When Z is negligible, so that only the A_1 mode is present, evolution takes place on a slow ($O(\gamma)$) timescale, while Z itself evolves at a rate independent of γ. We term these different types of dynamics the slow and fast phases, respectively. As we shall show below, it is possible to analyse the equations by matching together in a very simple way the behaviour in the two phases; it will emerge that the details of the bifurcation structure are independent of γ when the latter is small, and thus the description of the dependence of the solutions on the parameters is greatly simplified. In addition, the slow phase can be described analytically, while in the fast phase the small $O(\gamma)$ terms can be ignored, so that there are no stiffness problems with numerical computation. The techniques used are similar to those applied by Hughes & Proctor (1990*a*, *b*). The end result of the calculation is the reduction of the dynamics to that of a one-dimensional map,

representing the relation between extrema of the variable X. When $\Phi = 0$, equations (1.6) describe the case of conservative interactions. This special case has been extensively investigated in the case of small γ by Hughes & Proctor (1990*a*) and we shall therefore concentrate here exclusively on non-zero values of Φ. Preliminary results are contained in Proctor & Hughes (1990).

In §2 we locate the fixed points of equations (1.6), consider their stability and briefly discuss the regimes where bounded solutions are to be found. In §3 we describe how the solutions of equations (1.6) may be expressed in terms of a one-dimensional map relating certain minima of X. The map turns out to be multi-modal, with important implications for the existence and stability of multiple solutions occurring for the same parameter values. The properties of the map are discussed in §4 which also contains comparisons between solutions obtained directly from the map and those obtained by numerical solution of (1.6).

Hughes & Proctor (1990*a*) showed, for $\Phi = 0$, that for certain values of γ and δ the variable Z could become exceedingly small and that in such cases the addition of a small amount of random noise to the Z equation has a significant influence on the resulting solutions. The effect of such noise (which would certainly be present in a real fluid) was modelled by a straightforward change in the map. For non-zero Φ similar behaviour persists — the influence of noise and the consequent changes to the map are discussed in §5.

2. The fixed points and their stability

The origin is obviously a fixed point of equations (1.6) and is unstable for $\gamma > 0$. Other fixed points of the system are located at

$$X = -1, \quad Y = \tfrac{1}{2}\delta + \gamma\left(\frac{\tan\Phi + \tfrac{1}{2}\delta}{2 - \delta\tan\Phi}\right) + O(\gamma^2), \quad Z = \frac{\gamma(2 + \tfrac{1}{2}\delta^2)}{\cos\Phi(2 - \delta\tan\Phi)} + O(\gamma^2) \tag{2.1a}$$

and

$$X = -1, \quad Y = \cot\Phi + O(\gamma), \quad Z = \frac{2\cot\Phi - \delta}{\sin\Phi} + O(\gamma). \tag{2.1b}$$

Obviously Φ must be non-zero for the second of these fixed points to exist. Furthermore, since Z is positive by definition (see equation (1.5)) a necessary condition for the existence of both non-trivial fixed points when γ is small is that $\cos\Phi(2 - \delta\tan\Phi) > 0$. The stability of these points may be found by examining the growth rates σ of linearized disturbances. These are given as the roots of the cubic

$$[\sigma(\sigma - \gamma) + 2Z\cos\Phi](\sigma - \gamma + 2) = (\delta - 4Y)[\sigma(2Y - \delta) - 2Z\sin\Phi], \tag{2.2}$$

where Y and Z take their respective values from (2.1*a*, *b*). Analysis of this equation reveals that the fixed point (2.1*b*) is always unstable while the condition for the other fixed point (2.1*a*) to be stable is (correct to $O(\gamma)$)

$$2/\delta > \tan\Phi > \frac{2(4 - \delta^2)}{\delta(12 + \delta^2)}. \tag{2.3}$$

At the upper bound the fixed point ceases to exist; at the lower bound it loses stability in a Hopf bifurcation.

The fixed points of the reduced system (1.6) may be interpreted in terms of the amplitudes $A_{1,2}$ as a travelling wave with constant phase speed. Figure 1 shows

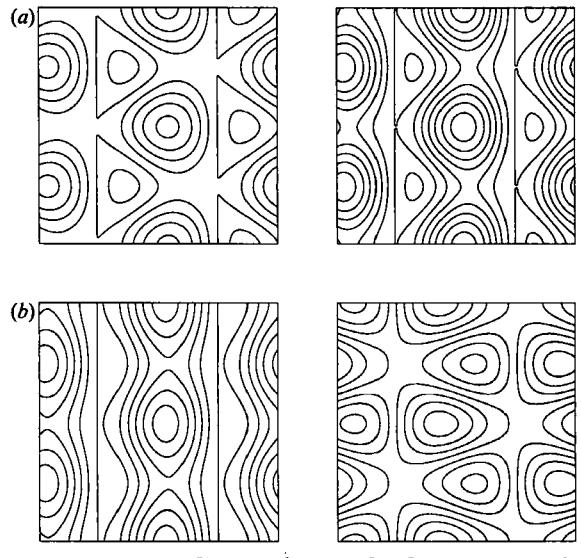

FIGURE 1. Wave patterns corresponding to the two fixed points given by (2.1*a*, *b*) for $\gamma = 0.1$, $\delta = 1$ and (*a*) $\Phi = 1$, (*b*) $\Phi = -0.2$.

contour plots of the spatial form of the waves for two different parameter values in the special case $\boldsymbol{k}_1 = (1,0)$, $\boldsymbol{k}_2 = (\frac{1}{2},\frac{1}{2})$, $\boldsymbol{k}_3 = (\frac{1}{2},-\frac{1}{2})$ and $\omega_2 = \omega_3$; the phase speed is then $2(\omega_2 + Y)$, with Y given by (2.1). Other more complex solutions of (1.6) (periodic orbits, chaotic solutions) represent patterns that travel at non-uniform velocity and whose amplitudes vary in time (see §6).

When $\cos\Phi < 0$, inspection of equations (1.6) reveals that the solutions are unbounded. As X decreases through negative values ($X < -1$), Z increases (from (1.6*c*)) and thereby accelerates the increase in $|X|$ through (1.6*a*). Furthermore, for $\frac{1}{2}\pi > \Phi > \tan^{-1}(2/\delta)$, when the fixed point (2.1*a*) no longer exists, the solutions are unbounded, as indeed they are for $-\frac{1}{2}\pi < \Phi < \Phi_c$ for some (negative) Φ_c dependent on δ. Precisely where bounded solutions are to be found will be discussed in more detail later. Since our aim in the present paper is to describe solutions that can be obtained by neglecting cubic terms, we shall from now on only concern ourselves with Φ in the region $\Phi_c < \Phi < \tan^{-1}(2/\delta)$.

3. Reduction to a one-dimensional map

As described in §1, when γ is small the dynamics of (1.6) is conveniently treated by separating the episodes of fast and slow evolution and then joining them together to yield a one-dimensional map relating specific extrema of the variable X (cf. Hughes & Proctor 1990*a*). When describing the dynamics for non-zero Φ (and in contrast to the case of $\Phi = 0$) it is best to deal first with the fast phase – this may end in one of three ways and it is instructive to consider these before tackling the slow phase. The fast phase is characterized by X, Y and Z being of order unity, and the terms involving γ therefore being negligible; unfortunately, except for the special case of $\Phi = 0$ it is not possible to obtain helpful analytic solutions of these equations. In the slow phase, on the other hand, Z is very small and X and Y evolve on an $O(\gamma^{-1})$ timescale. An important feature is that when Φ is non-zero the fast phase is not guaranteed to have bounded solutions; if $|X|$ is too large (X too negative) at the beginning of the fast phase then the trajectory escapes to infinity. Although it is not

possible to obtain a general expression for these critical values of X in terms of δ and Φ, it is possible to make considerable analytic headway for the case of small Φ; this is the topic of the following subsection. In §3.2 we study the fast phase in more detail when it *is* bounded. It turns out that there are two possible endings of the bounded fast phase and that these have a marked influence on the slow phase that follows – this stage of the evolution is considered in §3.3. A full discussion of the map that results from piecing together the fast and slow phases in contained is §4.

3.1 *The fast phase for small non-zero* Φ

3.1.1. *The reduced equations*

The existence, for $\Phi \neq 0$, of the unstable fixed point (2.1*b*) suggests that the fast phase will not be attracting if the starting point is sufficiently far from the origin. Although no general theory is available, it is possible to make analytic progress when $|\Phi| \ll 1$. In this limit the fixed point (2.1*b*) has $Z \sim 2\Phi^{-2}$, $Y \sim \Phi^{-1}$, which suggests the following scalings:

$$|\Phi| = \epsilon, \quad X = \epsilon^{-1}\tilde{X}, \quad Y = \epsilon^{-1}\tilde{Y}, \quad Z = \epsilon^{-2}\tilde{Z}, \quad \frac{\partial}{\partial t} = \epsilon^{-1}\frac{\partial}{\partial \tilde{t}}. \tag{3.1}$$

As mentioned above, since we are investigating the fast phase we would wish to be able to drop the terms in γ. For consistency, then, we must require that $\gamma \ll |\Phi|$ in all that follows. Substituting expressions (3.1) into equations (1.6), and dropping the tildes, we obtain, correct to $O(\epsilon)$,

$$\dot{X} = -2Y^2 + Z + \epsilon\delta Y, \tag{3.2a}$$

$$\dot{Y} = 2XY + \epsilon(-\delta X \pm Z), \tag{3.2b}$$

$$\dot{Z} = -2XZ - 2\epsilon Z, \tag{3.2c}$$

where the sign in (3.2*b*) is that of Φ. The resulting system is completely integrable for $\epsilon = 0$, with the conserved quantities

$$E = X^2 + Y^2 + Z, \quad C = YZ. \tag{3.3}$$

It is easy to see that the surfaces $E =$ constant, $C =$ constant intersect in closed curves so that the orbits are periodic. When $\epsilon \neq 0$ then trajectories will no longer be periodic and E and C will evolve slowly according to

$$\dot{E} = \epsilon(\pm 2YZ - 2Z), \tag{3.4a}$$

$$\dot{C} = \epsilon(-\delta XZ \pm Z^2 - 2YZ). \tag{3.4b}$$

Applying standard averaging techniques and defining a slow time $T = \epsilon t$, these become

$$E_T = \pm 2C - 2\langle Z \rangle, \tag{3.5a}$$

$$C_T = -\delta\langle XZ \rangle \pm \langle Z^2 \rangle - 2C, \tag{3.5b}$$

where the angle brackets indicate averages over the periodic orbit of the integrable system. The averages may be calculated when $\epsilon = 0$, giving

$$\langle XZ \rangle = -\tfrac{1}{2}\langle \dot{Z} \rangle = 0; \tag{3.6}$$

$$\langle Z^2 \rangle = E\langle Z \rangle - \langle X^2 Z \rangle - \langle Y^2 Z \rangle, \tag{3.7}$$

where

$$\langle Y^2 Z \rangle = \tfrac{1}{2}\langle Z^2 \rangle - \tfrac{1}{2}\langle \dot{X} Z \rangle, \tag{3.8}$$

and

$$\langle X^2 Z \rangle = -\tfrac{1}{2}\langle X\dot{Z} \rangle = \tfrac{1}{2}\langle \dot{X} Z \rangle. \tag{3.9}$$

Thus from (3.7), using (3.8) and (3.9),

$$\langle Z^2\rangle = \tfrac{2}{3}E\langle Z\rangle. \tag{3.10}$$

Using (3.6) and (3.10) in (3.5) we obtain finally

$$E_T = \pm 2C - 2\langle Z\rangle, \tag{3.11a}$$

$$C_T = -2C \pm \tfrac{2}{3}E\langle Z\rangle, \tag{3.11b}$$

where $\langle Z\rangle$ is to be evaluated as a function of C and E. It is interesting that δ does not enter the analysis until $O(\epsilon^2)$. Furthermore (3.11) is invariant under the transformation $\Phi \to -\Phi$, $E \to E$, $C \to -C$, so that we may take $\Phi > 0$ in what follows. We emphasize, however, that this indifference to the sign of Φ does not persist when $|\Phi| = O(1)$.

3.1.2. *Analysis of the reduced equations*

The quantity $\langle Z\rangle$ may be expressed in terms of elliptic integrals, the details being given in the Appendix. It is shown there that provided $K = C^2/E^3 \leqslant \frac{4}{27}$,

$$\langle Z\rangle = E\int_{h_1}^{h_2} \frac{h\,\mathrm{d}h}{(h^2-h^3-K)^{\frac{1}{2}}} \Big/ \int_{h_1}^{h_2} \frac{\mathrm{d}h}{(h^2-h^3-K)^{\frac{1}{2}}}, \tag{3.12}$$

where h_1 and h_2 are the positive zeros of denominator. It is in fact easy to show, by the following arguments, that K must indeed be less than or equal to $\frac{4}{27}$. From the definitions of E and C we obtain the following simple inequalities:

$$E = \langle X^2\rangle + \langle Y^2\rangle + \langle Z\rangle \geqslant \langle Y^2\rangle + \langle Z\rangle, \tag{3.13a}$$

while

$$C^2 = \langle YZ\rangle^2 \leqslant \langle Y^2\rangle\langle Z^2\rangle. \tag{3.13b}$$

Now from (3.2a) with $\epsilon = 0$, $\langle Z\rangle = \langle 2Y^2\rangle$, so that

$$E \geqslant \tfrac{3}{2}\langle Z\rangle, \quad C^2 \leqslant \tfrac{1}{2}\langle Z\rangle\langle Z^2\rangle = \tfrac{1}{3}E\langle Z\rangle^2, \tag{3.14}$$

giving $C^2 \leqslant 4E^3/27$ as required. For points on the boundary of the domain, equality must hold, so $E = \frac{3}{2}\langle Z\rangle$, $C^2 = \frac{1}{3}E\langle Z\rangle^2$. There is thus a fixed point when $\langle Z\rangle = C = 2$, $E = 3$, corresponding (in the limit $\Phi \to 0$) to the fixed point (2.1b) of the full equations. It may also be checked that when $C^2 = 4E^3/27$,

$$2CC_T = \tfrac{4}{9}E^2E_T = \tfrac{8}{9}CE^2 - 4C^2, \tag{3.15}$$

so that the boundary is in fact a trajectory of the system (3.11). If $C > 2$, $E > 3$ then C and E increase, while if $0 < C < 2$, $E < 3$ or $C < 0$ then $|C|$ and $|E|$ both decrease along the boundary.

Other trajectories of the system must be found by evaluating the integrals numerically and then integrating equations (3.11) by a time-stepping procedure. The results are shown in figure 2. Note that trajectories in $C < 0$ all approach the axis $C = 0$. This appears to be a singular line, but since, for small K and fixed E, $\langle Z\rangle \sim 1/|\ln C|$ it is in fact reached in a finite time. The ordering breaks down near $C = 0$ and the small terms act to move C into the right-hand half plane. The dynamics for $C > 0$ depends on whether the trajectory lies above or below the separatrix that joins the E-axis to the fixed point $C = 2$, $E = 3$. This curve intersects the E-axis at $E = E_0 \approx 4.41$. Below the separatrix all trajectories tend to the origin, while above it solutions initially decrease in amplitude, but eventually escape to infinity. Figure 2 shows that if $E < 3$ initially, then the solution remains bounded for any initial C,

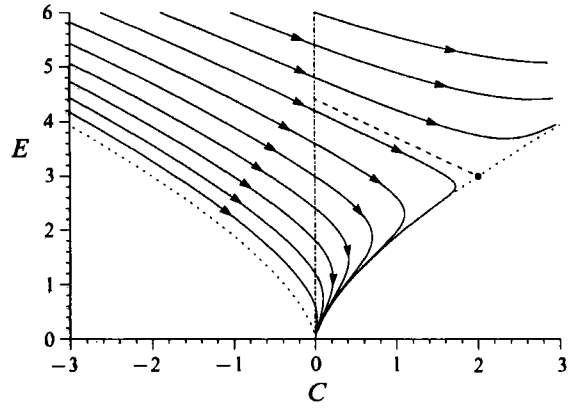

FIGURE 2. E versus C for the reduced system (3.11) with $\Phi > 0$. The dashed line is the curve $C^2 = 4E^3/27$. The fixed point (2, 3) and the separatrix curve are also shown.

while if we consider small starting values of C, such as will occur at the end of the slow phase, then E can be as large as E_0 without provoking runaway. In terms of the original variables this means that the boundary of runaway occurs when X^2+Y^2+Z is $O(\Phi^{-2})$.

As Φ increases, the solutions are only bounded if the initial values are within a diminishing neighbourhood of the origin. We have not investigated these restrictions for general Φ; when $\cos\Phi < 0$ the solutions are unbounded, as noted in §2, and in this case cubic terms will be required to produce bounded solutions. The above analysis demonstrates, however, that cubic terms are certainly not necessary for a range of values of the parameters.

3.2. *The attracting fast phase*

The analysis of the previous subsection showed that for small Φ, provided $|X|$ is not too large at the beginning of the fast phase, trajectories will be brought in towards the origin. The qualitative nature of this result holds also for larger values of Φ. Of course, the small Φ analysis cannot predict the detailed nature of the fast phase – in particular, it says that bounded solutions are attracted to $E = 0$, $C = 0$. In this subsection we examine the fast phase, when bounded, in more detail, paying particular attention as to exactly how it finishes. We now return to the original scaling of equation (1.6) and dispense with the restriction that $|\Phi| \ll 1$, which was in any case adopted in the last section only to permit analytical progress. Then at the end of the fast phase, which is governed by equations (1.6) with $\gamma = 0$, E tends to an $O(1)$ constant, E_1 say, and C tends to zero – in other words $X^2+Y^2 \to E_1$ and $Z \to 0$. The value of E_1 is of vital importance in determining the subsequent evolution.

If $E_1 > \frac{1}{4}\delta^2$ then $X \to X_0$ where $0 > X_0 > -1$ and $Y \to \frac{1}{2}\delta$. This behaviour is identical to that which occurs when $\Phi = 0$, and the subsequent slow phase is readily treated (see §3.3). It is worth pointing out again that when $\Phi \neq 0$, X_0 typically cannot be derived analytically but must be obtained from a numerical solution of (1.6) with $\gamma = 0$. The fast phase is deemed to have ended when the variation of E becomes sufficiently small and, as an additional check, when Z also is suitably small. (Our numerical integrations were performed until the ratio r of E at successive timesteps satisfied $|r-1| < 10^{-8}$ and until $Z < \exp(-200)$ – such an amazingly small value of Z may be obtained in numerical simulations by using $\ln Z$ instead of Z as the third dependent variable.)

If, on the other hand, $E_1 < \frac{1}{4}\delta^2$, then at the end of the fast phase trajectories do not tend to an invariant straight line, but tend instead to a circle that cannot intersect the line $Y = \frac{1}{2}\delta$. It is important to note that the fast phase can only end up with $E_1 < \frac{1}{4}\delta^2$ if Φ is negative. At the end of the slow phase (see §3.3) Y is close to, but slightly greater than $\frac{1}{2}\delta$. From (1.6*b*) it can then be seen that since Z is always positive then only if $\sin\Phi$ (and hence Φ) is negative can the trajectory be pushed across the $Y = \frac{1}{2}\delta$ line. The values of X and Y at the end of the fast phase become the starting point for the slow phase that follows. Not surprisingly, the evolution is rather different depending on whether E_1 is greater or less than $\frac{1}{4}\delta^2$ – the details are contained in the following subsection.

In terms of the fluid dynamical variables A_1, A_2 the fast phase represents the part of the cycle in which the linearly damped modes become significant and thus when the pattern deviates significantly from that of a uniform plane wave. These modes are destabilized only when the basic wave reaches a threshold amplitude, but they act to reduce the amplitude of the basic wave. It should be noted that in both the scenarios referred to above, the final amplitude $|A_1| \propto (X^2+Y^2)^{\frac{1}{2}}$ settles down to a constant value; the distinction between them is that in the former the phase of the damped modes is locked to that of the basic mode while in the latter there is a running phase.

3.3. *The slow phase*

3.3.1. $E_1 > \frac{1}{4}\delta^2$

If the fast phase finishes with $E_1 > \frac{1}{4}\delta^2$ then the subsequent slow phase is identical to that when $\Phi = 0$; we shall give a fairly brief, though self-contained, description below – full details may be found in Hughes & Proctor (1990*a*). The slow phase starts with Z small, $Y \approx \frac{1}{2}\delta$ and $X = X_0$ with $0 > X_0 > -1$. Throughout this stage of slow evolution, which takes place on a long ($O(\gamma^{-1})$) timescale, Z remains negligible with X negative and hence Y close to $\frac{1}{2}\delta$. If we write $Y = \frac{1}{2}\delta + \gamma\eta$ then, to leading order, X and η evolve according to the equations:

$$\dot{X} = \gamma X - \gamma\delta\eta, \tag{3.16a}$$

$$\dot{\eta} = \tfrac{1}{2}\delta + 2X\eta. \tag{3.16b}$$

Since X is negative and is evolving slowly it can be seen that $\eta \to -\delta/4X$, after a short initial transient, and hence from (3.16) X decreases according to the approximate equation

$$\dot{X} = \gamma\left(X + \frac{\delta^2}{4X}\right), \tag{3.17}$$

with Z varying according to (1.6*c*). If X_0 and X_1 (Z_0 and Z_1) are the values of $X(Z)$ at the beginning and end of the slow phase then these equations may be solved to give

$$\tfrac{1}{2}\gamma(\ln Z_0 - \ln Z_1) = f(X_1) - f(X_0), \tag{3.18}$$

where

$$f(X) = \int_0^X \frac{\xi(1+\xi)}{\xi^2 + \frac{1}{4}\delta^2}\,\mathrm{d}\xi = \tfrac{1}{2}\ln\left(1 + \frac{4X^2}{\delta^2}\right) + X - \tfrac{1}{2}\delta\tan^{-1}\left(\frac{2X}{\delta}\right). \tag{3.19}$$

Now, on input to the slow phase Z is of the order of some power of γ. It then decreases to a minimum at $X = -1$ and subsequently increases again as X continues to decrease. The slow phase is considered to end when the omitted Z term in (3.17) becomes significant; this occurs when $Z = O(\gamma)$. Hence, from (3.18),

$$f(X_0) = f(X_1) + O(\gamma|\ln\gamma|). \tag{3.20}$$

For negative X, $f(X)$ increases from zero, reaches a maximum at $X=-1$ and then decreases again. Thus if (3.20) is to be satisfied with $X_0 \neq X_1$ we must have $0 > X_0 > -1$ and $X_1 < -1$. To leading order (3.20) simply becomes

$$f(X_1) = f(X_0) \quad (X_1 \neq X_0). \tag{3.21}$$

Expression (3.21) is a good approximation to (3.20) except when X_0 (and hence X_1) is close to -1 when the $O(\gamma|\ln\gamma|)$ terms become important. When $\Phi = 0$, the fast phase brings trajectories close to the fixed point at $X=-1$ and it is imperative to derive a better approximation to the map in this region (see Hughes & Proctor 1990*a*). For Φ very small this is still true; however, for $\Phi \gtrsim O(\gamma)$, the case we are studying here, the fast phase never ends close to the fixed point and (3.21) is of sufficient accuracy.

3.3.2. $E_1 < \frac{1}{4}\delta^2$

If $E_1 < \frac{1}{4}\delta^2$ at the beginning of the slow phase then things are rather different. The variable $E (\approx X^2+Y^2$, since Z is small) evolves on the slow timescale γ^{-1} until Y becomes $\frac{1}{2}\delta$, the slowly spiralling trajectory hitting $Y=\frac{1}{2}\delta$ when X is very close to zero. From here onwards the slow phase behaves as described above, but in order to make use of (3.18), which determines the end of the slow phase, it is necessary to know the size of Z when Y becomes $\frac{1}{2}\delta$.

At the end of the fast phase Z is of the order of some power of γ (as we shall see, we do not need to be any more accurate than this). Hence, from (1.6), X and Y evolve according to the approximate equations

$$\dot{X} = \gamma X + \delta Y - 2Y^2, \tag{3.22a}$$

$$\dot{Y} = \gamma Y - \delta X + 2XY, \tag{3.22b}$$

and hence $\dot{E} \approx 2X\dot{X} + 2Y\dot{Y} \approx 2\gamma E$. At the beginning of the slow phase $E = E_1$ and at the transition point ($Y \approx \frac{1}{2}\delta$, $X \approx 0$) $E \approx \frac{1}{4}\delta^2$. Thus the duration of this stage is $\tau = (2\gamma)^{-1}\ln(\delta^2/4E_1)$; the concomitant decrease in Z can then be calculated using (1.6*c*). Since X is oscillating rapidly and symmetrically about $X=0$ then, over a long timescale, equation (1.6*c*) may be approximated by $\dot{Z} = -2Z$ and hence $[\ln Z] = [-2t]$. If $Z \sim \gamma^m$ at $t=0$ (the start of the slow phase) then if $Z = Z_0$ at $t=\tau$, to leading order we have

$$\gamma \ln Z_0 = -\ln(\delta^2/4E_1). \tag{3.23}$$

We now know the value of Z at the beginning of the usual slow phase where X and Y evolve according to (3.16). Hence from (3.18), using the fact that $X_0 \approx 0$, we have

$$f(X_1) = -\tfrac{1}{2}\ln\left(\frac{\delta^2}{4E_1}\right). \tag{3.24}$$

We are now in a position to construct the map relating extrema of X attained at the end of successive slow phases. It should be noted that although *some* computation is required, in order to determine the fast phase, a great saving is made on solving the full equations (1.6). In that case the majority of time is spent on integrating the equations during the slow phases – in the construction of the map it is precisely these portions that we can treat analytically.

4. Description of the map

It can be seen from the results of §3 that the maps we finally obtain, on combining the analytic results of the slow phase with the numerical calculations of the fast phase, are completely independent of γ, depending only on δ and Φ. (As

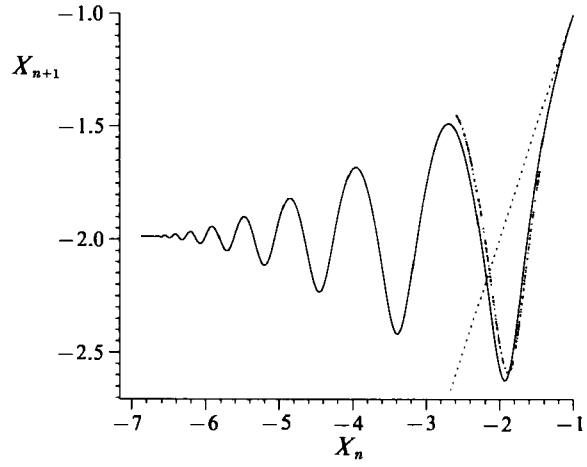

FIGURE 3. Calculated map for $\delta = 0.1$, $\Phi = 0.3$ (full line) compared with results of numerical simulations of the o.d.e.s. (1.6) with $\gamma = 10^{-2}$.

mentioned earlier, this condition is true provided that $\Phi \gtrsim O(\gamma)$ – for $\Phi \lesssim O(\gamma)$ an additional analysis is needed, as described by Hughes & Proctor 1990*a* for the case of $\Phi = 0$.) As noted in §1, without loss of generality we may restrict attention to positive values of δ but must consider both positive and negative values of Φ.

The description of the map when Φ is positive is relatively straightforward and so we shall consider this case first. Figure 3 shows the map obtained by plotting X_{n+1} versus X_n, where X_n denotes the minimum of X obtained at the end of the nth slow phase, for $\delta = 0.1$ and $\Phi = 0.3$. The map terminates abruptly, at $X = X_f$ say, when, as explained in §3, the value of $|X|$ at the end of the slow phase (beginning of the fast phase) is too large for the subsequent fast phase to be attracting and the trajectory escapes to infinity. The map takes on the form of a sequence of oscillations which decrease in amplitude as X decreases (when Φ is zero they are all of the same height). It can be seen that for the case depicted in figure 3 the right-most valley is attracting and that any trajectory started outside that range (but with $X > X_f$) will rapidly be drawn into this region, where it will forever remain. Thus, provided the initial values of X, Y and Z are not such as to cause the solution to become unbounded immediately then there is no possibility of this happening at a later time – indeed, this appears always to be true for positive Φ. Also shown on figure 3 are the minima of X at the end of the slow phases obtained from direct numerical solution of the ordinary differential equations (1.6) with $\gamma = 10^{-2}$. It can be seen that agreement with the map is excellent, a fact that allows us to discuss the properties of the map in detail, confident that it is a good approximation to the full system (1.6). Furthermore we see verification of the prediction of the map that all trajectories will be confined to the right-most valley.

As Φ is increased X_f increases, as shown by the sequence of plots in figure 4, and the number of oscillations is reduced. Furthermore the valleys of the map become less deep – in consequence the map cuts the diagonal ($X_{n+1} = X_n$) with a small gradient (between -1 and $+1$) and the fixed point of the map (for $X < -1$) becomes stable (see figure 4*c*). Recall that this fixed point of the map is not a fixed point of the differential equations, but corresponds to a periodic orbit. As Φ is increased yet further this fixed point moves closer to the fixed point at $X = -1$ (which *is* a fixed point of the o.d.e.s (1.6), being given by (2.1*a*)) until they meet. Stability is then

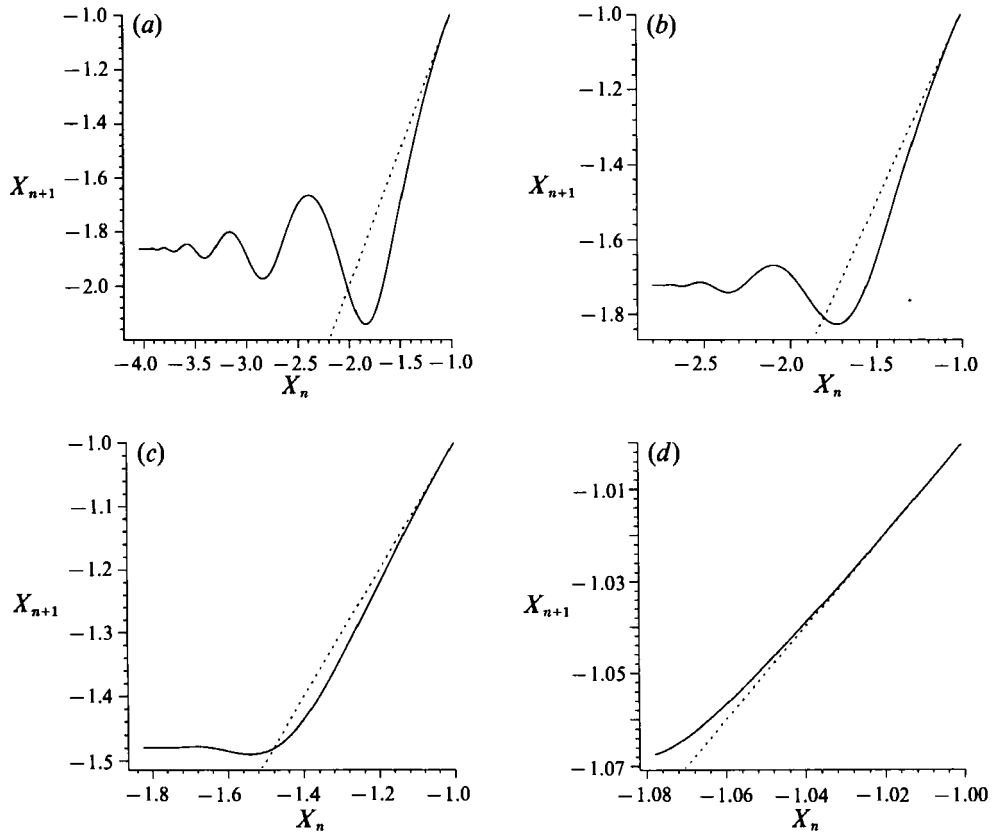

FIGURE 4. A sequence of maps for positive values of Φ with $\delta = 0.1$ (*a*) $\Phi = 0.5$; (*b*) $\Phi = 0.7$; (*c*) $\Phi = 1.0$; (*d*) $\Phi = 1.45$. As Φ increases the cutoff value X_f increases also. This leads to a stable fixed point (case (*c*)) which later collides with, and transfers stability to the origin (case (*d*)).

transferred to the fixed point at $X = -1$, the value of Φ at which this occurs being given by the lower bound in inequality (2.3). Then for a short range of Φ, with Φ satisfying inequality (2.3), the fixed point at $X = -1$ is stable (see figure 4*d*). However, for $\Phi \geqslant \tan^{-1}(2/\delta)$ there are no fixed points (see §2) and no bounded solutions of the o.d.e.s (1.6).

As δ is increased for a given Φ the undulations are pushed to the left until the entire map lies to the left of the diagonal and the fixed point at $X = -1$ is stable. When Φ and δ are such that inequality (2.3) is satisfied then the fixed point at -1 remains stable. When δ is increased above $2/\tan \Phi$ then there is no map, all trajectories of the original differential equations being unbounded.

The most striking feature of the maps illustrated in figures 3 and 4 is their multimodality, the presence of multiple extrema in the map. One of the key characteristics of such maps is the possible existence of several different stable orbits for the same parameter values, each orbit being reached by a sequence of interactions starting from different extrema of the map (see MacKay & Tresser 1987 for the theory of bimodal (two-humped) maps, and Hughes & Proctor 1990*a* for the occurrence of such a map in a physical system). As we shall see shortly, when Φ is negative such considerations are of tremendous importance; for Φ positive however, as illustrated by the maps of figure 4, we see that the behaviour is more straightforward. Orbits starting from any extremum are attracted into the right-most valley; the effective

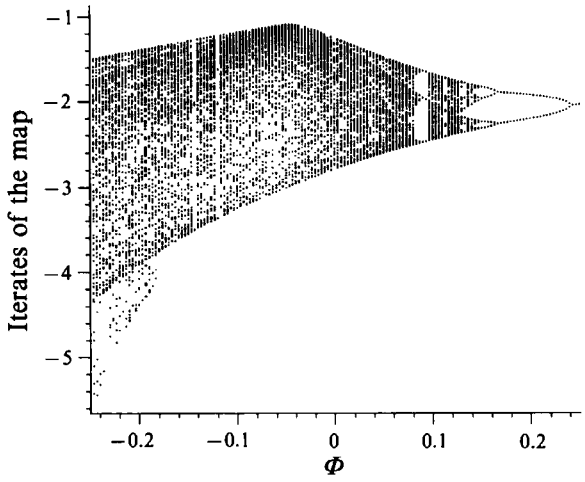

FIGURE 5. Bifurcation diagram constructed by plotting a sequence of iterates of the map (after the decay of transients) for a range of Φ with $\delta = 0.5$. The final iterate for one value of Φ is used as the starting value for the next, slightly different, Φ value.

map is therefore just single-humped and its properties are well known. As discussed above, the shape of the map is changed by varying Φ or δ (or a combination of the two). The clearest means of seeing the orbits that result as the map changes is to construct a bifurcation diagram by plotting a certain number of iterates of the map after any transient behaviour has died away. Figure 5 plots such iterates for a range of Φ (both positive and negative) at the fixed value of $\delta = 0.5$.

When Φ is negative the map displays more unusual properties. As discussed in §3, the quantity $E\,(= X^2 + Y^2 + Z)$ may now become less than $\frac{1}{4}\delta^2$ at the end of the fast phase, giving rise to an extended slow phase described by equation (3.24). When this occurs the valleys of the map become deeper, as shown by a comparison of (3.21) and (3.24), the equations describing the two types of slow phase. Furthermore, the valleys no longer decrease in depth monotonically with X. These features are displayed in figure 6 which plots the map for several negative values of Φ for $\delta = 0.5$ – the dashed portions of the curve denote those ranges of X for which the slow phase is protracted, described by (3.24). Now that valleys other than the right-most can dip below the diagonal there is the possibility of more than one stable periodic orbit for the same parameter values. This situations is illustrated in figure 6 (a) where δ and Φ are such that the minimum of the second valley lies on the line $X_{n+1} = X_n$ at $X \approx -3.9$. Obviously this extremum of the map is a stable (indeed superstable) fixed point. By contrast, an orbit starting from the right-hand minimum of the map is chaotic and can never reach the stable fixed point at the bottom of the second valley – this is illustrated by the sequence of iterations shown in figure 6 (a). Thus the nature of the solution depends crucially on the initial values of the variables. The influence of the second valley for $\Phi = -0.163$ is clearly seen in figure 5. Reassuringly, we have been able to confirm that this behaviour is indeed possessed by the o.d.e.s (1.6). Figure 7 (a, b) plots X versus time, determined from numerical solution of (1.6) with $\gamma = 10^{-3}$, corresponding to the two possible orbits of figure 6 (a). From the fluid mechanics point of view, we can associate the appearance of additional attractors with the possibility of temporal intermittency.

As Φ is decreased below its value in figure 6 (a) the valleys become deeper, with the consequence that orbits starting from the second minimum no longer remain in the

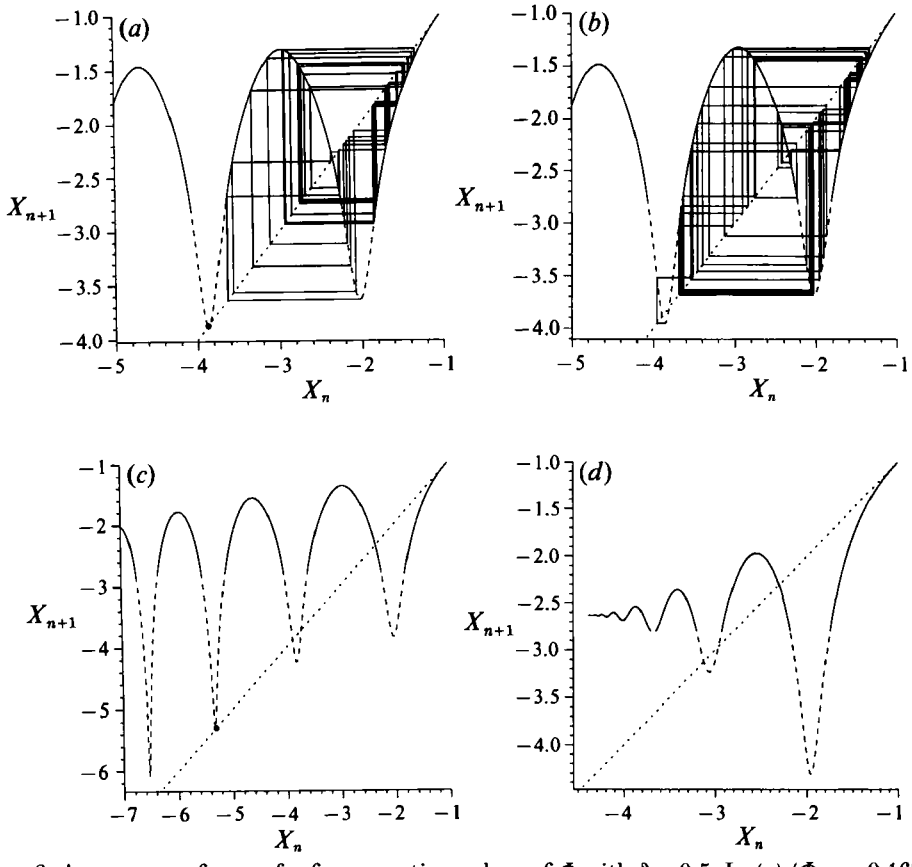

FIGURE 6. A sequence of maps for four negative values of Φ with $\delta = 0.5$. In (*a*) ($\Phi = -0.163$) the bottom of the second valley represents a superstable fixed point; in (*b*) ($\Phi = -0.17$) trajectories from the second valley are attracted into the first valley; in (*c*) ($\Phi = -0.191$) the third valley meets the diagonal giving rise to a new superstable fixed point; in (*d*) ($\Phi = -0.5$) Φ is sufficiently negative for the right-most valley to have become the deepest. The solid lines denote the end of the slow phase started with $E_1 > \frac{1}{4}\delta^2$; the dashed lines correspond to the protracted slow phase with starting value $E_1 < \frac{1}{4}\delta^2$.

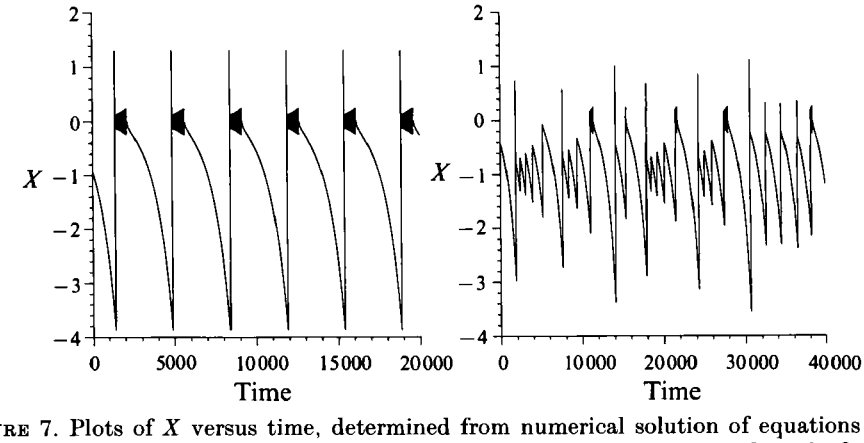

FIGURE 7. Plots of X versus time, determined from numerical solution of equations (1.6) with $\gamma = 10^{-3}$, corresponding to the two possible orbits of figure 6 (*a*). (*a*) corresponds to the fixed point of the map (the dark sections denote the extended slow phase in which $X^2 + Y^2$ varies slowly, but with X oscillating extremely rapidly); (*b*) shows the chaotic orbit associated with the right-most valley.

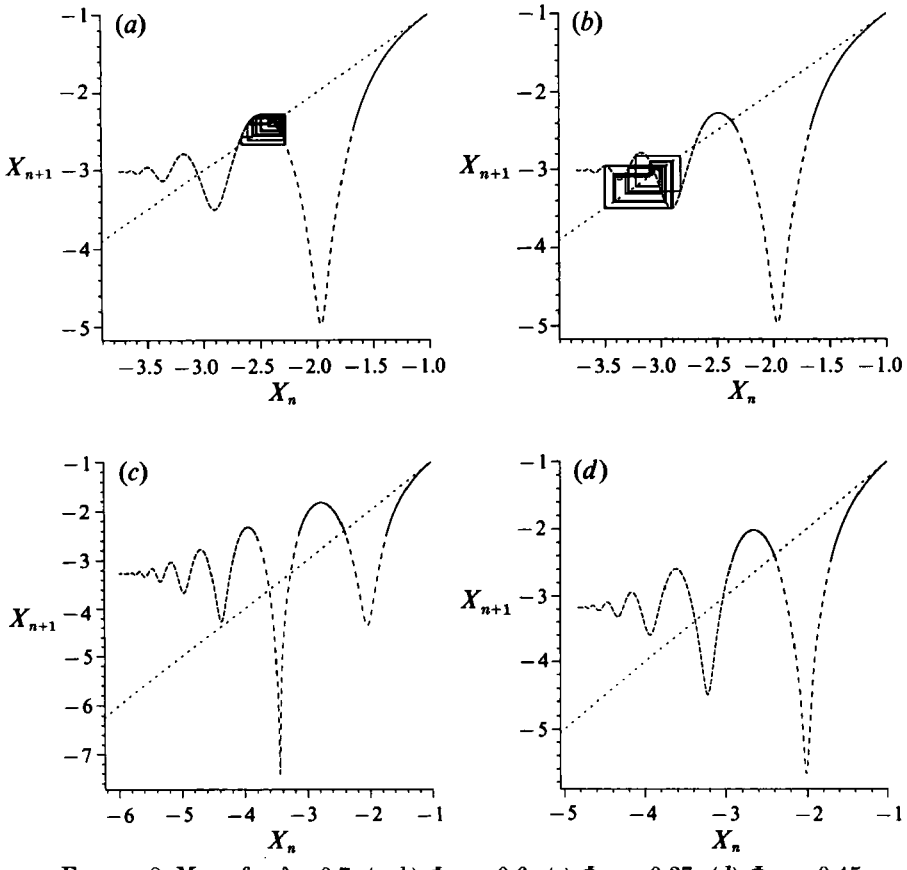

FIGURE 8. Maps for $\delta = 0.7$. (*a*, *b*) $\Phi = -0.6$; (*c*) $\Phi = -0.37$; (*d*) $\Phi = -0.45$.

neighbourhood of that point but are instead attracted to the rightmost valley (figure 6*b*). However, as Φ is decreased yet further the third valley comes below the diagonal, thus introducing another superstable fixed point (figure 6*c*). We do not expect to find the (co-dimension 3) situation where there are three superstable orbits since the map depends only on the two parameters δ and Φ. The relationship between the shape of the map and the value of Φ is a complicated one when Φ is negative. Further decreases in Φ below its value in figure 6(*c*) eventually reduce the depth of the second and 'higher' valleys, leaving the rightmost valley the deepest (figure 6*d*).

The deepening of the valleys for negative Φ also has another significant consequence. As can be seen from figure 8, certain minima of the maps are less than the cutoff value X_f and, in such cases, an orbit through one of these minima will escape on the next iteration since the map has no image for that point. However, by no means all orbits will escape; figures 8(*a*, *b*) illustrate that even for maps where escape is a possibility there exist bounded orbits which steer well clear of the deep valley. Thus we have the interesting feature that orbits from certain starting values will escape to infinity whereas orbits from others will remain bounded for all times. Furthermore, the boundary separating these two classes of starting values is complicated and parts of it are almost certainly of a fractal nature. Figure 9 plots an 'escape diagram' for a range of starting values of X and a range of Φ – the different shades of grey reflect the time taken for the solution to escape from that particular

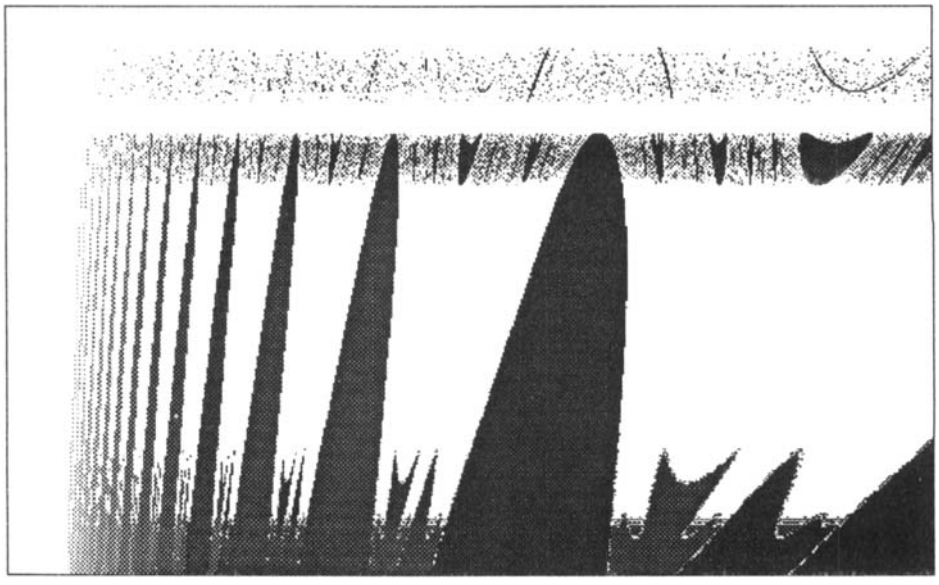

FIGURE 9. Grey-scale plot showing the tendency for solutions to escape; $\delta = 0.7$. The abscissa is the range of starting values plotted logarithmically from $X = -1$ (on the left) to $X = -3$; the ordinate is the parameter Φ, plotted linearly, from $\Phi = -0.3$ (at the top) to $\Phi = -0.9$. Each starting point is iterated up to 16 times: the white regions denote starting values whose iterates have not escaped in this time; the black region denotes points that escape immediately; the grey regions intermediate escape times.

starting point, with the darkest shades denoting the most rapid escape. By construction, each region corresponding to escape in n iterations possesses a pre-image, corresponding to escape in $n+1$ iterations. This accounts for the self-similar nature of the structure in the horizontal direction. There are also two horizontal bands of note. In the upper band ($-0.35 \gtrsim \Phi \gtrsim -0.4$) the second valley, but not the first, is deeper than the cutoff and allows escape (see Figure 8*c*); the valley however is extremely narrow and thus relatively few orbits reach the bottom of the valley and escape. For Φ in the interval $-0.4 \gtrsim \Phi \gtrsim -0.43$ none of the valleys of the map is deeper than the cut-off and there is no escape. For $-0.43 \gtrsim \Phi \gtrsim -0.48$ trajectories can escape from the first (rightmost) valley; furthermore, the map allows re-injection of trajectories back into the first valley from the left (see figure 8*d*) and thus produces a fairly complicated escape pattern. For $\Phi \lesssim -0.48$ solutions again escape from the first valley; now however there is no re-injection of orbits and the escape pattern is more straightforward. This picture provides a clear illustration of the unpredictable nature of the effect of resonant terms in nonlinear wave interactions and shows how difficult it would be to describe what is happening simply from repeated numerical simulations of the governing equations. It also makes plain the considerable advantages of reducing the system to a one-dimensional map.

5. The influence of noise

All physical systems are, to some extent, affected by external disturbances or noise. Often, when the noise level is low, the effect is correspondingly small – the resultant behaviour is then only slightly modified from that in the absence of noise and there is no need to include the effect of noise in the governing equations. For the

example considered here, however, the situation is somewhat different, with a small ($O(\epsilon)$) amount of noise having a significant ($O(1)$) effect.

In the absence of any noise, when the system is described by equations (1.6), orbits approach the invariant plane $Z = 0$ very closely when γ is small. If perturbations to the system act so as to 'kick' trajectories away from this plane then the value of Z at the beginning of the slow phase may be altered and, from (3.18), the value of X at the end of the slow phase will then be affected also. In order for $O(\epsilon)$ disturbances of Z to have an $O(1)$ effect on X it can be seen from (3.18) that $\gamma \ln \epsilon$ should be $O(1)$. Thus in the case of small γ, the noise level of significance is truly tiny, being $O(\exp(-1/\gamma))$. Since the key effect of any noise on the system is to perturb Z we need only include additive noise in equation (1.6*c*) with (1.6*a*, *b*) remaining unchanged. Recalling from (1.5) that Z is a positive definite quantity we introduce a new variable W, with $Z = W^2$, and replace (1.6*c*) by

$$\dot{W} = -W(1+X)+\epsilon h(t), \tag{5.1}$$

where $h(t)$ is some stationary random process with zero mean. The noise term will only be of significance during the slow phase, when $|W|$ (and hence Z) is small; during the fast phase W is $O(1)$ and the noise may then be neglected. The most rigorous approach to the problem is to formulate a Fokker–Planck equation for the probability distribution of W during the slow phase, and hence for the value of X at the end of the slow phase (see Stone & Holmes 1990; Hughes & Proctor 1990*b*). On combining the slow phase with the fast phase (where the noise is negligible) we may obtain a conditional probability distribution for the value of X at the end of the $(n+1)$th slow phase given the value of the extremum at the end of the nth slow phase. In the limit of $\gamma \to 0$ this probability distribution becomes sharply peaked about the expected value of the extremum and it is then appropriate to incorporate the relation between the expected values of successive extrema into a modified version of the map described in §§3 and 4. The Fokker–Planck analysis however is somewhat lengthy and so here we shall derive the amended map, taking into account the influence of noise, from the more heuristic approach of Hughes & Proctor (1990*a*). The two approaches do of course agree in the limit of small γ.

In the absence of noise the variable Z initially decreases in the slow phase, reaching a minimum at $X = -1$ before increasing as X decreases through -1. To a first approximation the effect of additive noise in (5.1) is to prevent $|W|$ from falling below the level of the noise, which we shall take to be $O(\epsilon)$. Thus if, in the noise-free evolution, $Z \gtrsim O(\epsilon^2)$ the influence of the noise will be unimportant. On the other hand, if $Z < O(\epsilon^2)$ with no noise then the addition of noise will be significant; in particular, $|W|$ will be constantly perturbed so as to remain $O(\epsilon)$ for $X > -1$ before growing as X decreases through -1. The important feature is that $|W|$ at the start of its growth phase is larger than in the absence of noise and consequently the value of $|X|$ at the end of the slow phase, governed by (3.18), will be smaller. In equation (3.18) we may thus take $Z_0 = K\epsilon^2$, $X_0 = -1$ and $Z_1 = O(\gamma)$ to yield the following expression for X_1, the value of X at the end of the slow phase:

$$f(X_1)-f(-1) = -\alpha+O(\gamma|\ln\gamma|), \tag{5.2}$$

where $\alpha = \gamma|\ln\epsilon|$ is assumed to be $O(1)$. The precise value of the $O(1)$ constant K is obviously immaterial. It can be seen from the above argument that to the first degree of approximation it is only the level of the noise that is important and not its distribution – in other words we do not need to take account of the exact form of the function $h(t)$ in (5.1).

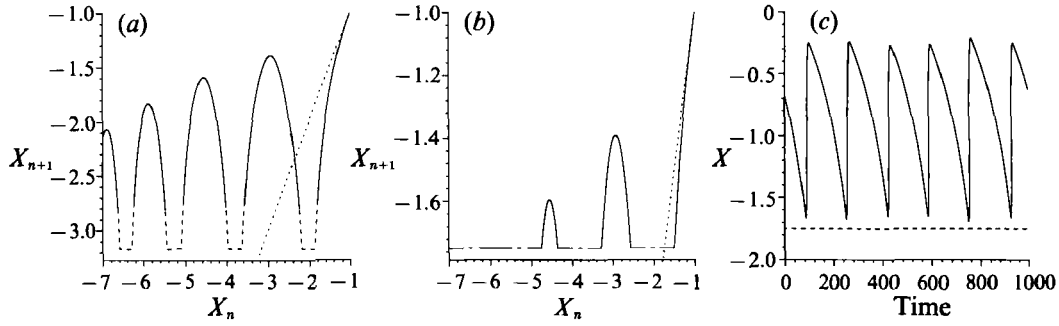

FIGURE 10. (a, b) show maps flattened by the inclusion of noise; $\delta = 0.5$, $\Phi = -0.2$. (a) $\alpha = -\gamma \ln \epsilon = 1.0$; (b) $\alpha = 0.1842$. (c) plots X versus time, calculated from the o.d.e.s (1.6), with $\gamma = 10^{-2}$ and $\epsilon = 10^{-8}$, corresponding to case (b). The mean maximum amplitude predicted from the map is marked as the dashed line.

The prescription for incorporating the effects of noise into the map is thus straightforward. To a first approximation we may regard the modified map as deterministic even though it models the effects of noise on the differential equations. Numerical experiments do of course reveal fluctuations about the mean represented by the map but these appear to be of secondary importance and, in any case, their standard deviation becomes very small in the limit $\gamma \to 0$ with $\gamma|\ln \epsilon|$ fixed. At the end of the slow phase we choose the *greater* value of X between that given by (3.21) (or (3.24) if $E_1 < \frac{1}{4}\delta^2$) and that given by (5.2). As can be seen from figure 10(a) the result is that the valleys of the map now have a flat cutoff. Thus for given parameter values there will be some orbits that are influenced by noise – those sampling the flat regions – whilst there might be others that are restricted to the noise-free sections. (These latter orbits are not entirely unaffected by noise; for example, gaps may appear in period-doubling sequences (see Crutchfield, Farmer & Huberman 1982). However, such effects, while not covered by our approach, are small compared to the significant changes in trajectories resulting from the flattened map.) A small amount of external noise, represented by the modified map, thus leads to an entirely different bifurcation structure (see Proctor & Hughes 1991). If the noise is sufficiently large that the flat part of the map intersects the diagonal (see figure 10b), then the map has a stable fixed point and the system of o.d.e.s has a (noisily) periodic orbit with amplitude controlled by the noise. Further increases in the noise level simply act to reduce the amplitude of the orbit. Thus the effect of additive noise is, somewhat counter-intuitively, to make the solutions more ordered. The flat sections of the map allow for periodic orbits with a large basin of attraction and, in consequence, many orbits that are chaotic in the absence of noise become (noisily) periodic. Furthermore, the raising of the valley floors is a deterrent to escaping orbits and indeed, a sufficiently high level of noise will ensure that all orbits are constrained.

Figure 10(c) shows the good agreement between the solution of the o.d.e.s ((1.6a,b), (5.1)) and the mean amplitude predicted from the map; for computational purposes we take $h(t)$ in equation (5.1) to be normally distributed with standard deviation $(\mathrm{d}t)^{\frac{1}{2}}$ for a timestep $\mathrm{d}t$, thus ensuring results independent of the timestep. As pointed out above, when γ is small only a very slight amount of noise is needed to influence the solutions; for example if $\gamma = 10^{-2}$ and $\alpha = 1$ then $\epsilon = \exp(-100)$. Typically, when solving differential equations numerically, a greater level of noise than this will be introduced, albeit unwillingly, through rounding errors. For our particular problem, however, described by equations (1.6), we are fortunate in being

able to produce effectively noise-free solutions (as displayed in figure 7, for example) by working with the variable $V = \ln Z$ in (1.6*c*) and introducing V into (1.6*a*, *b*) only when it is greater than some critical value.

6. Discussion

In this paper we have considered the interaction of three resonant waves, one linearly unstable and two equally damped, with non-conservative quadratic nonlinearities; to facilitate analytic progress we assumed the growth rate of the unstable mode to be very small in comparison with the damping of the other modes. Since the phenomenon of non-conservative three-wave resonance will arise in many situations where small-amplitude disturbances can exchange energy with a mean flow we have chosen to keep our discussion of a general nature rather than highlight any particular physical problem. Indeed, evaluating the coefficients Γ_i, Δ_i in equation (1.2) for a given flow is by no means straightforward, as shown by Craik (1971) (see also Usher & Craik 1974) who derived equations for the resonant interaction between a two-dimensional wave C_1 and two oblique modes $C_{2,3}$ imposed on a parallel shear flow.

The reduction of the governing equations to a one-dimensional map relating certain extrema of X greatly clarifies the behaviour of the system. Forming iterates of the map for a range of parameter values leads to a bifurcation diagram of the form of figure 5; certain features, such as the locations of periodic orbits and transitions to chaos are then readily found. Furthermore, consideration of the map allows us to state precisely how many stable solutions to expect for any given parameter values and also allows us to calculate rapidly whether given initial conditions will lead to a bounded solution. In addition we have included the effects of a small amount of random noise in the equations by a suitable modification of the map.

The change of variables (1.5) is important in that it reduces an ostensibly fourth-order system to the third-order system (1.6). However, to relate the results to wave interactions in fluids it is necessary to consider the modulus and phase of A_1 and A_2. With the same choice of $\mathbf{k}_i$ and ω_i as in figure 1, the wave pattern viewed in a frame moving in the positive x-direction with speed $2\omega_2$ takes the form

$$f(x, y) = |A_1| \cos(x + \phi_1) + 2|A_2| \cos(\tfrac{1}{2}x + \phi_2) \cos \tfrac{1}{2}y. \tag{6.1}$$

For almost all the time $|A_2|$ is negligible; the wave pattern is essentially planar and travels at relative speed δ. The fast phase represents bursting behaviour of the oblique modes leading to a drastic alteration in the wave pattern. Two examples of the evolution of a burst are shown in figure 11. The imposition of noise reduces both the maximum amplitude of the bursts and the intervals between them. Of course in a real experiment the wave patterns would be much less regular, but we believe that the above calculations give a useful guide as to what might be observed.

Finally we comment on the neglect of the cubic terms in the governing equations (1.6). Clearly, if the equations yield bounded solutions for all sufficiently small initial amplitudes then the neglect of small cubic terms (which preserve the invariance of the plane $Z = 0$) is justified. This is the case for positive Φ, provided that $\tan \Phi < 2/\delta$, and some negative values of Φ. However, for Φ sufficiently large and negative we can achieve a situation like that depicted in figure 9 where certain starting values lead to bounded solutions whereas others escape to infinity. 'Good' and 'bad' starting values are interleaved in a complex manner; yet in certain cases (e.g. $\Phi = -0.5$ in figure 9) the good values dominate. In this circumstance one should

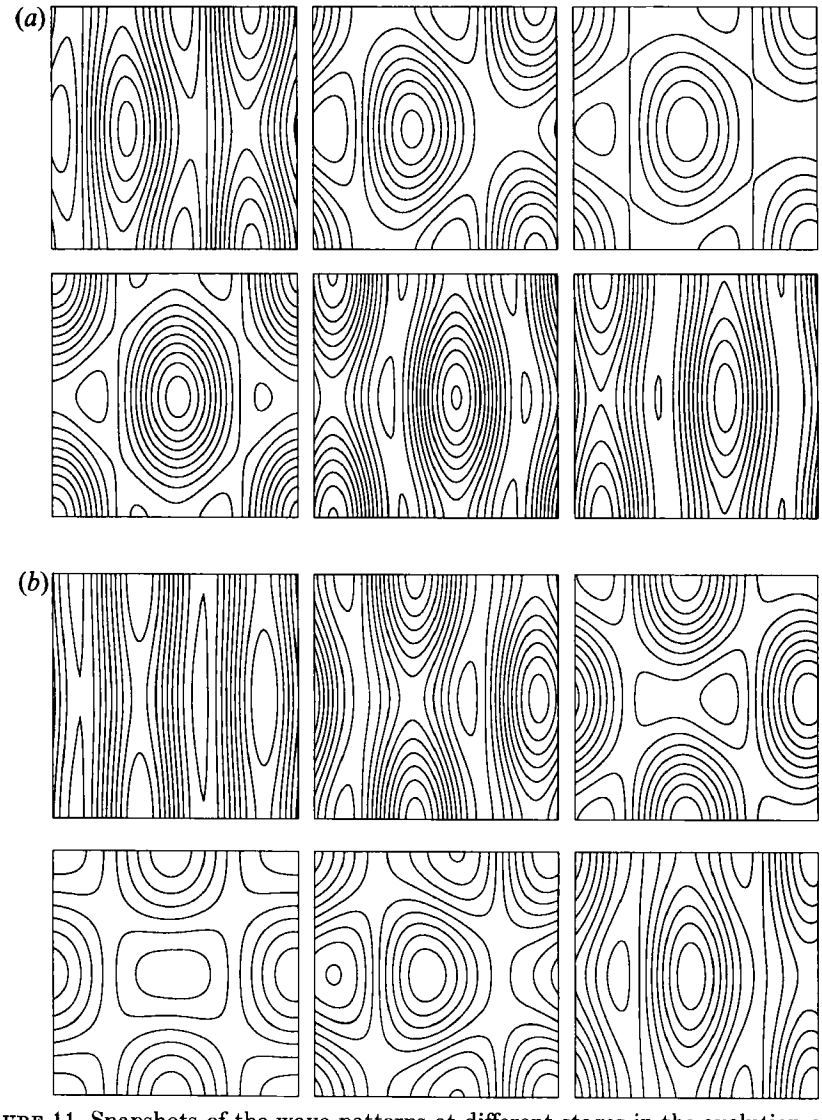

FIGURE 11. Snapshots of the wave patterns at different stages in the evolution of a burst. $\gamma = 10^{-3}$, $\delta = 0.5$ and (*a*) $\Phi = 0.2$, (*b*) $\Phi = -0.2$.

perhaps include cubic terms for a proper solution whilst recognizing that in many cases these will be redundant. The role of the quadratic terms in exchanging energy with the mean flow remains somewhat obscure. Indeed it can easily be shown that if all the linear growth/decay rates are zero then all solutions with $Z \neq 0$ blow up (for small enough δ) for small Φ of either sign. Computations indicate that for finite Φ only negative values of Φ lead to a significant extraction of energy from the basic state and the blow up of initially small solutions. Clearly the mechanism by which this occurs is complicated, depending in a non-trivial manner on the phase relationship between the three modes.

We are grateful to Trinity College, Cambridge and the Science and Engineering Research Council for financial support.

Appendix

In this Appendix we explain how $\langle Z \rangle$ may be expressed as a ratio of elliptic integrals, leading to the result (3.12).

On making the substitution

$$X = E^{\frac{1}{2}} \sin\theta \cos\phi, \quad Y = E^{\frac{1}{2}} \sin\theta \sin\phi, \quad Z = E \cos^2\theta, \tag{A 1a–c}$$

we find that for $\epsilon = 0$, from (3.2c),

$$2E\dot{\theta} \sin\theta \cos\theta = 2E^{\frac{3}{2}} \sin\theta \cos^2\theta \cos\phi. \tag{A 2}$$

From (3.3), $C = YZ = E^{\frac{3}{2}} \sin\theta \cos^2\theta \sin\phi$ = constant and hence we may write (A 2) as

$$2\dot{\theta} \sin\theta \cos\theta = 2E^{\frac{1}{2}} \sin\theta \cos^2\theta [1 - K/(\sin^2\theta \cos^4\theta)]^{\frac{1}{2}}, \tag{A 3}$$

where $K = C^2/E^3$ = constant, Writing $h = \cos^2\theta$, expression (A 3) becomes

$$|\dot{h}| = E^{\frac{1}{2}}(h^2 - h^3 - K)^{\frac{1}{2}}, \tag{A 4}$$

for $h_1 \leqslant h \leqslant h_2$, where h_1 and h_2 are the positive zeros of the quantity in brackets. Then average of Z is given by

$$\langle Z \rangle = \int_{h_1}^{h_2} \frac{Z}{|\dot{h}|} \mathrm{d}h \Big/ \int_{h_1}^{h_2} \frac{\mathrm{d}h}{|\dot{h}|}, \tag{A 5}$$

which, on using (A 1c), leads to the result (3.12).

REFERENCES

Busse, F. H. 1984 Transition to turbulence via the statistical limit cycle route. In *Turbulence and Chaotic Phenomena in Fluids* (ed. T. Tatsumi), pp. 197–202. North-Holland, Amsterdam.

Craik, A. D. D. 1968 Resonant gravity-wave interactions in a shear flow. *J. Fluid Mech.* **34**, 531–549.

Craik, A. D. D. 1971 Nonlinear resonant instability in boundary layers. *J. Fluid Mech.* **50**, 393–413.

Craik, A. D. D. 1985 *Wave Interactions and Fluid Flows.* Cambridge University Press.

Crawford, J. D. & Knobloch, E. 1991 Symmetry and symmetry-breaking bifurcations in fluid dynamics. *Ann. Rev. Fluid Mech.* **23**, 341–87.

Crutchfield, J. P., Farmer, J. D. & Huberman, B. A. 1982 Fluctuations and simple chaotic dynamics. *Phys. Rep.* **92**, 45–82.

Hughes, D. W. & Proctor, M. R. E. 1990*a* Chaos and the effect of noise in a model of three-wave mode coupling. *Physica* D **46**, 163–176.

Hughes, D. W. & Proctor, M. R. E. 1990*b* A low-order model for the shear instability for convection: chaos and the effect of noise. *Nonlinearity* **3**, 127–153.

Knobloch, E. & Proctor, M. R. E. 1988 The double Hopf bifurcation with 2:1 resonance. *Proc. R. Soc. Lond.* A**415**, 61–90.

MacDougall, S. R. & Craik, A. D. D. 1991 Blow-up in non-conservative second-harmonic resonance. *Wave Motion* **13**, 155–165.

MacKay, R. S. & Tresser, C. 1987 Some flesh on the skeleton: the bifurcation structure of bimodal maps. *Physica* D **27**, 412–422.

Phillips, O. M. 1981 Wave interactions – the evolution of an idea. *J. Fluid Mech.* **106**, 215–227.

Proctor, M. R. E. & Hughes, D. W. 1990 Chaos and the effect of noise for the double Hopf bifurcation with 2:1 resonance. In *Nonlinear Evolution of Spatio-Temporal Structures in Dissipative Continuous Systems* (ed. F. H. Busse & L. Kramer), pp. 375–384. Plenum.

Proctor, M. R. E. & Hughes, D. W. 1991 The false Hopf bifurcation and noise sensitivity in bifurcations with symmetry. *Eur. J. Mech.* B *Fluids* **10** (2) Suppl., 81–86.

STONE, E. F. & HOLMES, P. 1990 Random perturbation of heteroclinic attractors. *SIAM J. Appl. Maths* **50**, 726–743.

USHER, J. R. & CRAIK, A. D. D. 1974 Nonlinear wave interactions in shear flows. Part 1. A variational formulation. *J. Fluid Mech.* **66**, 209–221.

VYSHKIND, S. YA. & RABINOVICH, M. I. 1976 The phase stochastization mechanism and the structure of wave turbulence in dissipative media. *Sov. Phys, J. Exp. Theor. Phys.* **44**, 292–299.

WANG, P. K. C. 1972 Bounds for solution of nonlinear wave-wave interacting systems with well-defined phase description. *J. Math. Phys.* **13**, 943–947.

WEILAND, J. & WILHELMSSON, H. 1977 *Coherent Nonlinear Interaction of Waves in Plasmas.* Pergamon.

WERSINGER, J.-M., FINN, J. M. & OTT, E. 1980 Bifurcation and 'strange' behaviour in instability saturation by nonlinear three-wave mode coupling. *Phys. Fluids* **23**, 1142–1154.